Journal of Alloys and Compounds 509 (2011) 10132–10138

Contents lists available at SciVerse ScienceDirect

Journal of Alloys and Compounds

journal homepage: www.elsevier.com/locate/jallcom

Preparation and characterization of platinum doped porous titania nanoparticles for photocatalytic oxidation of carbon monoxide

R.M. Mohamed [a,b,*], Elham S. Aazam [a]

[a] Chemistry Department, Faculty of Science, King Abdulaziz University, Jeddah, Saudi Arabia
[b] Nanostructured Materials Division, Advanced Materials Department, Central Metallurgical R&D Institute, Helwan, 11421, Cairo, Egypt

ARTICLE INFO

Article history:
Received 6 June 2011
Received in revised form 11 August 2011
Accepted 12 August 2011
Available online 22 August 2011

Keywords:
Mesoporous titania Pt nanoparticles
Template self assembly
Characterization
CO photocatalysis

ABSTRACT

TiO_2 samples doped with platinum oxide were obtained by using a sol–gel low temperature approach. The photocatalytic oxidation of CO in the presence of O_2 was monitored to study the influence of the Pt doping on the photocatalytic degradation performance of TiO_2. The obtained results were compared with those obtained with TiO_2 Degussa (P-25). Photocatalytic studies of the prepared mesoporous Pt/TiO_2 nanoparticles for the photooxidation of CO revealed notable photocatalytic activity, which was 3 times higher than that of Pt photodeposited onto commercial TiO_2 Degussa P-25. Also quantum yield for CO_2 formation for mesoporous Pt/TiO_2 calcined at 500 °C is higher than that of Pt photodeposited onto commercial TiO_2 Degussa P-25 by about three times. The structure and textural properties Pt/TiO_2 were studied by X-ray powder diffraction (XRD), N_2 adsorption (BET), Transmission electron microscopy (TEM) and UV.

1. Introduction

One of the most active areas in environmental research is the development of highly efficient methods for the elimination of hazardous pollutants from air, soil and water. The semiconductor photocatalysis is recognized as one of the promising techniques for this purpose. The photocatalytic activity of semiconductors is observed when electrons and the corresponding positive holes are generated in the conduction and valence band of the semiconductors respectively, as a result of UV irradiation [1].

Nanocomposite composed of semiconductor oxides and noble metals has found important applications in catalysis and the generation of photocurrent and photovoltage. In particular, TiO_2 coupled with noble metals, such as Pt, Pd, Au, or Ag, has been served as excellent visible-light photocatalysts [2–17] or CO oxidation catalysts [18–20].

It is well known that TiO_2 adsorbed with noble metals can improve the efficiency of electron-transfer dynamic and also enhance the efficiency of photocatalytic redox processes [21–24].

Titanium dioxide (TiO_2) is a very important semiconducting photosensitive material, which has undergone extensive investigation over the past two decades owing to its many outstanding physicochemical properties [25]. In particular, photoinduced reactivity of and photocatalytic activity of various TiO_2 phases have been widely investigated and utilized in many technological applications such as dyesensitized solar cells, water-splitting, synthesis of organic compounds, and decomposition/degradation of organic pollutants etc. [25].

For example, TiO_2 is a well-known UV absorbing transition-metal oxide and the bulk anatase TiO_2 has a direct transition optical band gap of 3.2 eV. When it works as a catalyst in photocatalysis under ultraviolet (UV) light irradiations, the charge separation between the photon-generated carriers becomes a crucial factor in determining the ultimate catalytic performance of TiO_2 catalysts [25]. In order to increase its surface area and thus light absorbing ability, TiO_2 has been coated or deposited onto different types of support materials or carriers.

Being a model reaction, the photocatalytic oxidation of CO using platinized TiO_2 has been studied by many scientists [26,27]. It is well known that Pt deposits on TiO_2 not only increase the photo-induced electron transfer rate at the interface but also provide catalytic sites. Hwang et al., concluded that Pt nanoparticles deposited on TiO_2 in enhancing the CO photooxidation rate provides surface sites on which active oxygen species photogenerated from adsorbed O_2 are stabilized [26]. Vorontsov et al., found that CO photocatalytic activity increases with lowering of Pt oxidation state (highest with Pt^0/TiO_2) [27]. Gan et al. observed that both TiO_2 surface structure and Pt nanocluster size have profound effects on CO surface chemistry [27]. Photocatalysis is an environmentally friendly method for CO oxidation since such a system can operate at ambient temperatures under clean and abundant solar light irradiation. TiO_2 as a photocatalyst has been applied for a variety

* Corresponding author at: Chemistry Department, Faculty of Science, King Abdulaziz University, Jeddah, Saudi Arabia. Tel.: +966 540715648.
E-mail address: redama123@yahoo.com (R.M. Mohamed).

0925-8388/$ – see front matter © 2011 Elsevier B.V. All rights reserved.
doi:10.1016/j.jallcom.2011.08.059

of environmentally interesting operations regarding water and air purification [28–32].

This work deals with the synthesis of highly ordered hexagonal mesoporous Pt/TiO_2 nanocomposites via a sol–gel approach. Such method is a non-expensive and versatile approach that allows us to synthesize a great variety of crystalline inorganic oxides, at low temperature. The texture properties, structure and composition of the catalyst prepared were characterized by N_2 adsorption, UV–vis absorption spectra, XRD and Transmission electron microscope (TEM). Finally, the photocatalytic oxidation of CO in the presence of O_2 was monitored to study the influence of the Pt doping on the performance of degradation of TiO_2. Our results were compared with those obtained using the commercial TiO_2 Degussa P25.

2. Experimental

2.1. Reagents

All chemicals used were of analytical reagent grade (Sigma Chemical Reagent Company) as described below:

Triblock copolymer Pluronic P123, titanium tert-butoxide $Ti(OC(CH_3)_3)_4$(TBOT), HCl, C_2H_5OH, and H_2PtCl_6 and TiO_2 Degussa P-25.

2.2. Preparation method

2.2.1. Preparation of Pt/TiO_2 nanoparticles (Pt-500, Pt-600, and Pt-700)

The synthesis of platinum-doped TiO_2 was achieved with a sol–gel approach. Triblock copolymer pluronic P123 was used as structure directing agent, for a typical synthesis, in a first step, triblock copolymer Pluronic P123 (1.5 g) was dissolved in a mixture solution of deionized water (20 mL), 2 M HCl (7 g) and C_2H_5OH (12.1 g). In a second step, a calculated amount of H_2PtCl_6 (0.6 wt% Pt/TiO_2) is poured while stirring at 35 °C to a solution of TBOT (3.5 g). After stirring the resulting mixture subjected to a moderate hydrogen atmosphere at 35 °C for 24 h, then aged without stirring under H_2 atmosphere at 80 °C for another 24 h. As Final step, the polymer template P123 was removed during calcination since the samples were calcined at 500, 600 and 700 °C in air for 5 h to remove the surfactant and to obtain highly ordered mesostructured PtO/TiO_2 product. Subsequently, the Pt/TiO_2 samples were subjected to H_2 gas for 2 h at 400 °C to obtain Pt/TiO_2 samples. The obtained Pt-doped TiO_2 samples were labeled (Pt-500, Pt-600, and Pt-700) depending on the calcinations temperature.

2.2.2. Preparation of Pt/TiO_2 Degussa

TiO_2 Degussa (P-25) was mixed with H_2PtCl_6 solution containing the equivalent amount of Pt to obtain 0.6 wt% Pt/TiO_2 Degussa P-25.

The mixture was magnetically stirred for 24 h under UV illumination. After irradiation the sample was centrifuged, washed and dried at 110 °C overnight. The as-synthesized product was calcined at 500 °C in air for 5 h to obtain Pt/TiO_2 Degussa. Subsequently, the Pt/TiO_2 Degussa sample was subjected to H_2 gas for 2 h at 400 °C to obtain Pt/TiO_2 Degussa (Pt-25).

2.3. Characterization

The textural properties of the samples were evaluated from the adsorption–desorption isotherms of nitrogen at −196 °C detected using a Nova2000 series apparatus (Chromatech). The specific surface areas of the materials were calculated using the BET method within a 0.005–0.30 range of relative pressure (P/P^0). Prior to detection, the samples were degassed under vacuum at 270 °C for 5 h. X-ray diffraction analysis was performed using a Rigaku RINT, 2000, CuKα radiation, λ = 0.15406 nm). Diffuse reflectance ultraviolet–visible absorption spectra (DRS UV–vis) were collected in the UV–vis range (200–800 nm) with $BaSO_4$ as reference on a Shimadzu UV-2450 spectrophotometer at 22 °C. The morphologies and particle sizes of the prepared samples were examined with a transmission electron microscope (Hitachi H-9500 operated at 300 kV).

2.4. Photocatalytic evaluation

Photocatalytic properties of the samples were evaluated following the photooxidation of CO. Experiments were carried out in a cylindrical glass reactor (35 mm diameter and 120 mm length) that contains a UV xenon lamp source (150 W and medium pressure) placed inside a quartz jacket and equipped with a cooling tube as illustrated in Fig. 1.A feed gas of ca. 400 ppmV was made up of CO (purity 99.99%) and air, and was stored in a high-pressure cylinder.

For all the experiments, the photocatalyst weight was fixed at 0.2 g of either mesoporous Pt/TiO_2 or Pt/TiO_2 Degussa (Pt-25) was placed into catalyst cell which composed from three quartz layers, first layer to allow the gas mixture to pass, second layer to put catalyst inside it and third layer to allow the gas mixture only to out.

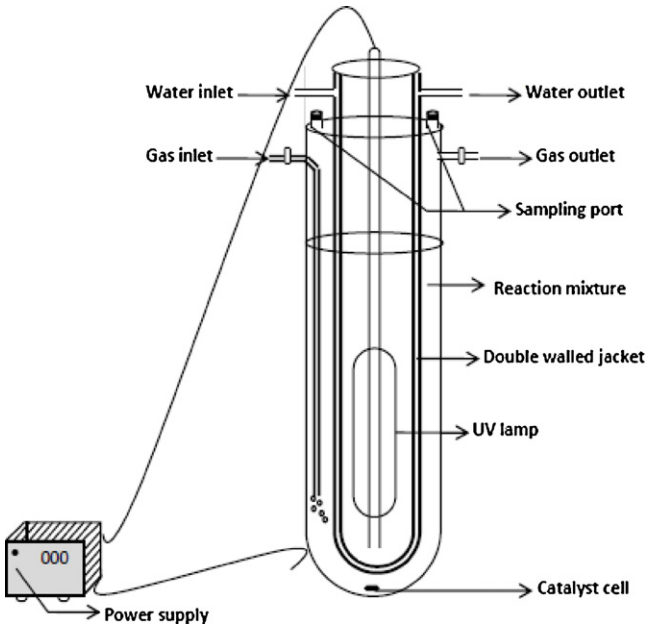

Fig. 1. Schematic representation of a typical photoreactor.

The gas entered the reactor as withdrawn at regular intervals from the upper part of the reactor via a gas-sampling valve, so that the photocatalyst was homogeneously dispersed at all times.

The change of CO concentration was determined by chromatographic method (Shimadzu GCMS-QP 5050A).

The removal efficiency of CO was calculated adopting the following equation:

$$\%\ \text{Removal efficiency} = \frac{C_0 - C}{C_0} \times 100$$

where C_0 is the original CO content and C is the retained CO.

The photonic efficiency was calculated for each experiment as the ratio of the CO_2 formation rate and the incident light intensity as given in the following equation.

$$\xi = \frac{r \times 100}{I}$$

where ξ is the photonic efficiency (%), r the photooxidation rate of CO, and I the incident photon flux (3.37×10^{-6} Ein L^{-1} s^{-1}).

The quantum yield of CO_2 formation could be determined as $\Phi = \xi/F_s$, where ξ is photonic efficiency and F_s is the fraction of light observed by tested catalyst [33].

3. Results and discussion

3.1. Characterization of the catalysts

3.1.1. Assessment of surface areas of Pt/TiO_2 nanocomposites

The values of specific surface areas, S_{BET} ($m^2\ g^{-1}$) of the concerned systems were calculated by applying BET equation, total pore volume V_p ($mL\ g^{-1}$) which is the volume of liquid nitrogen adsorbed at relative pressure very close to saturation [$P/P^0 = 0.99$], the total pore volume is a measure of total porosity of the solid catalyst which are cited in Table 1, and Fig. 2.

Following up the displayed results, one would resolve these features:

1- The isotherms show hysteresis loops in the range of mesopores with a clear step in the isotherms [34]. All the isotherms in Fig. 2 have different hysteresis loops and areas, generally; the desorption branch joins the adsorption one at ∼1.The turn over at the top indicate the presence of mesopores.
2- The hysteresis loops for Pt-500, Pt-600 and Pt-700 approaching type IV, which is usually associated with the filling and emptying of the mesopores by capillary condensation.

Table 1
Textural and photocatalytic properties of Pt/TiO_2 (Pt-500, Pt-600, Pt-700 and Pt-25) and pure P-2.

Photocatalysts	S_{BET} ($m^2\ g^{-1}$)	P_{TiO2} (nm)	P_{Pt} (nm)	Total V_p (cm^3/g)	Quantum yield (Φ)
Pt-500	284	6	12	0.49	0.0160
Pt-600	251	8	17	0.35	0.0905
Pt-700	183	9	20	0.30	0.0954
Pt-25	178	10	10	0.24	0.0304
Pure P-25	120	10	–	0.15	0.0215

Surface area (S_{BET}), average particle size of TiO_2 nanoparticle (P_{TiO2}), average particle size of Pt nanoparticle (P_{Pt}) and total pore volume (V_p).

3- With respect to Pt-500 and Pt-600, raising the calcination temperature from 500 to 600 °C is accompanied by decrease in the measured S_{BET} values as shown in Table 1 with increasing the crystallite size [35,36]. The drop in the surface areas as observed upon raising the calcination temperature from 500 to 700 °C can be understood taking into account sintering effect which increases with increase calcination temperature.
4- For Pt-600 the hysteresis loop is broader and shifts to higher relative pressure (Fig. 2b). This broadening and shifting indicates some loss in long-range ordering of the mesopores and the hysteresis loop can instead be interpreted as resulting from the voids between non-ordered particles. The main pore sizes increased to 8, 9 nm upon calcination of the Pt/TiO_2 nanocomposites to 600 and 700 °C, respectively. Finally, in order to make a comparative study with Pt/TiO_2 Degussa (Pt-25), a nitrogen adsorption isotherm for Pt-25 was studied (Fig. 2d), the results show that a typical type II adsorption isotherm is found for Pt-25 [37], which indicate that the pore structure is complex and tend to made up of interconnected networks of pores.

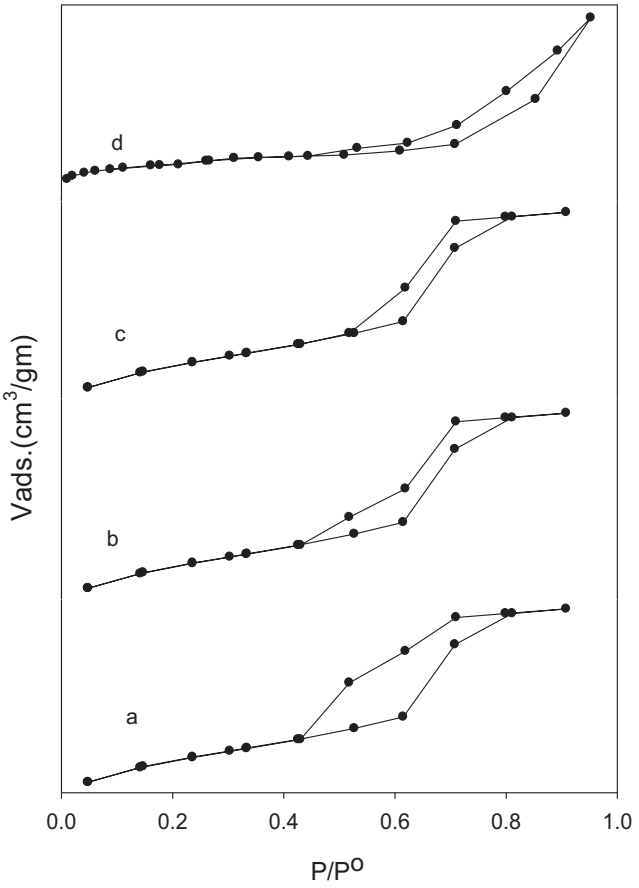

Fig. 2. N_2 adsorption isotherms of Pt-500 (a), Pt-600 (b), Pt-700 (c) and Pt-25 (d).

3.1.2. X-ray diffraction

In order to investigate the phases of the final product, XRD patterns the systems under consideration were studied. Fig. 3(a) and (b) shows the low and long angle XRD pattern respectively for Pt/TiO_2 as prepared and calcined systems.

Inspection of the obtained XRD diffractograms as given in Fig. 3A would reveal the following:The low angle and wide angle XRD patterns of prepared samples are presented in Fig. 3a and b, respectively. The low angle peak appeared ($2\theta = 2.3°$) in all samples indicate that the formation of ordered structure in mesoporous scale [38].For the uncalcined sample, the observed high intensity and sharpness of the peak prove that a long-range order exists in the Pt/TiO_2 nanocomposite. However, upon increasing the calcination temperature the diffraction peaks are becoming weaker, thus referring to a reduction of the long-range ordering of the mesopores.

Compared to Fig. 3a for low angle XRD, Fig. 3b wide angle XRD ($2\theta = 10–80°$) reveal that an amorphous crystal structure which diminished with increasing calcinations temperature, since Pt-600 ant Pt-700 nanocomposite detected showing reflections from a typical anatase TiO_2 phase with characteristic diffraction peaks at 2θ equal to 25.2, 38, 48, 54–55, 63 and 69–70 and 75–76° [39].

The diameter D of TiO_2 is estimated by applying the Scherer's equation [40,41] as follows:

$$D = \frac{57.3k\lambda}{\beta\cos\theta} \quad (1)$$

where k is the particle shape factor (generally 0.9), λ is the wavelength of Cukα1 radiation (0.1541 nm), β is the calibrated half intensity width of the selected diffraction peak (degrees), θ is the Bragg angle (half of the peak position), D is the particle diameter and the factor 57.3 is used to convert β in degree to radian measurement from Eq. (1).

The average diameter of the TiO_2 is calculated. For Pt_{600} and Pt_{700} is about 8 and 9 nm respectively as tabulated in Table 1, indicating that larger TiO_2 anatase particles have been formed at this higher calcination temperature (Table 1). It is evident that after the collapses of some of the hexagonal ordering the pore channels themselves start to collapse and disordered mesostructures of crystalline TiO_2 are obtained.

3.1.3. TEM analysis

Fig. 4 shows TEM images of Pt/TiO_2 as prepared (Degussa) and the calcined Pt/TiO_2 ($Pt_{500–700}$ °C).

It can be observed in the TEM image pertaining to Degussa Fig. 4d that, Pt nanoparticles with diameters ranging between 12 and 20 nm.

Interestingly, TEM images for the calcined part Fig. 4(a)–(c) indicated that, almost Pt nanoparticles are not located on the outer surface and their growing creates new pores by destructing part of the channels wall.

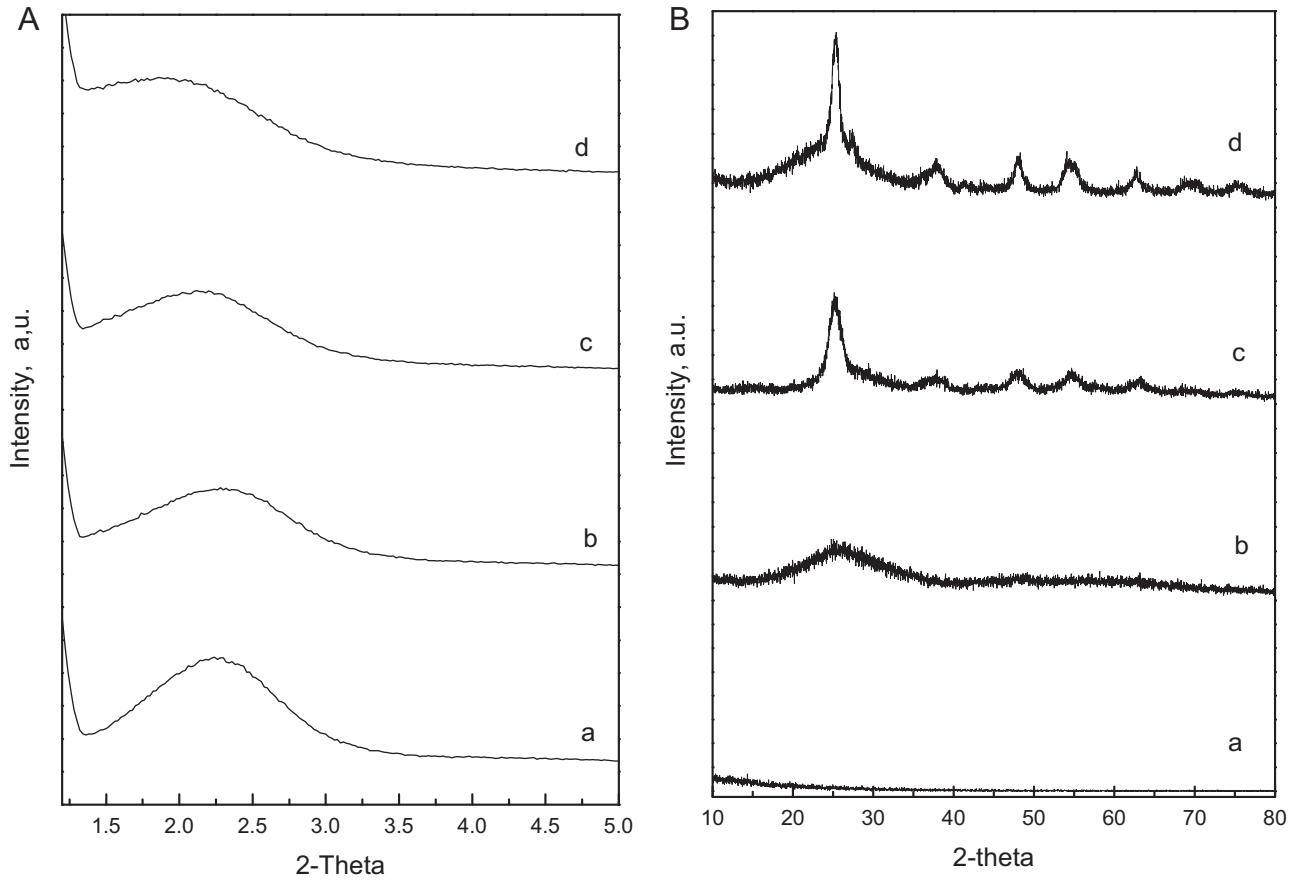

Fig. 3. (A) Low angle XRD patterns of uncalcined Pt/TiO_2 (a) Pt-500 (b), Pt-600 (c) and Pt-700 (d). (B) Long angle XRD patterns of uncalcined Pt/TiO_2 (a) Pt-500 (b), Pt-600 (c) and Pt-700 (d).

3.1.4. UV–vis spectroscopy

Fig. 5 shows the UV–vis absorption spectra of the calcined Pt/TiO_2 (Pt-500, Pt-600 and Pt-700 °C). It is clear from the figure that there is a significantly absorption in the visible region. The red shifted photo response of these systems may lead to a high photocatalytic activity which helps in the enhancement of photocatalytic activity.

The band gap energies were calculated by the equation:

$$E_g = \frac{1239.8}{\lambda}$$

where E_g is the band gap (eV) and λ (nm) is the wavelength of the absorption edges in the spectrum.

The band gap values of the calcined part (Pt-500, Pt-600 and Pt-700 °C) are given in Table 2. The band gap energy of Pt-25 and that of pure anatase are higher compared to that of the calcined Pt/TiO_2 (Pt-500, Pt-600 and Pt-700 °C).

For pure anatase, the significant increase in the absorption wavelength (λ) can be assigned to the intrinsic band gap absorption [38]. The band gap (E_g) is estimated to be 3.2 eV, which is in good agreement with the reported value for anatase (3.2–3.3 eV). The lower band gap of Pt/TiO_2 can enhance the photocatalytic activity.

Table 2
Direct band gap for Pt-500, Pt-600, Pt-700, Pt-25 and pure P-25.

Photocatalysts	Band gap (eV)
Pt-500	3.03
Pt-600	2.93
Pt-700	2.93
Pt-25	3.10
P-25	3.20

3.2. CO photocatalytic oxidation on Pt/TiO_2 catalysts

The catalytic oxidation of CO with O_2 is one of the simplest bimolecular surface reactions and often used as a model for the research of the photocatalytic-oxidation reaction [42,26,27]. The catalytic oxidation of CO by O_2 was investigated using a static system.

It is well known that the reaction rate of CO oxidation on platinum metals is of first order with respect to CO at low CO concentration. The effect of calcination temperature CO photocatalytic activity was investigated.

The photocatalytic efficiencies of the synthesized Pt/TiO_2 nanocomposites calcined at temperatures between 500 and 700 °C for the photooxidation of carbon monoxide to carbon dioxide were compared with that of Pt-25 and P-25.

Furthermore, the photocatalytic oxidation of CO% in relation to the irradiation time over the systems of Pt/TiO_2 photocatalysts and TiO_2 Degussa P-25 is graphically represented and compared in Fig. 6

The features emerge from the obtained results are as follows:

1. The reaction time required to completely remove CO (100%) was found to decrease from 55 to 35 min upon increasing the calcination temperature from 500 to 700 °C respectively, whereas % of photocatalytic oxidation of CO for Pt-25 and P-25 are 66.99 and 27.00% respectively after 60 min.

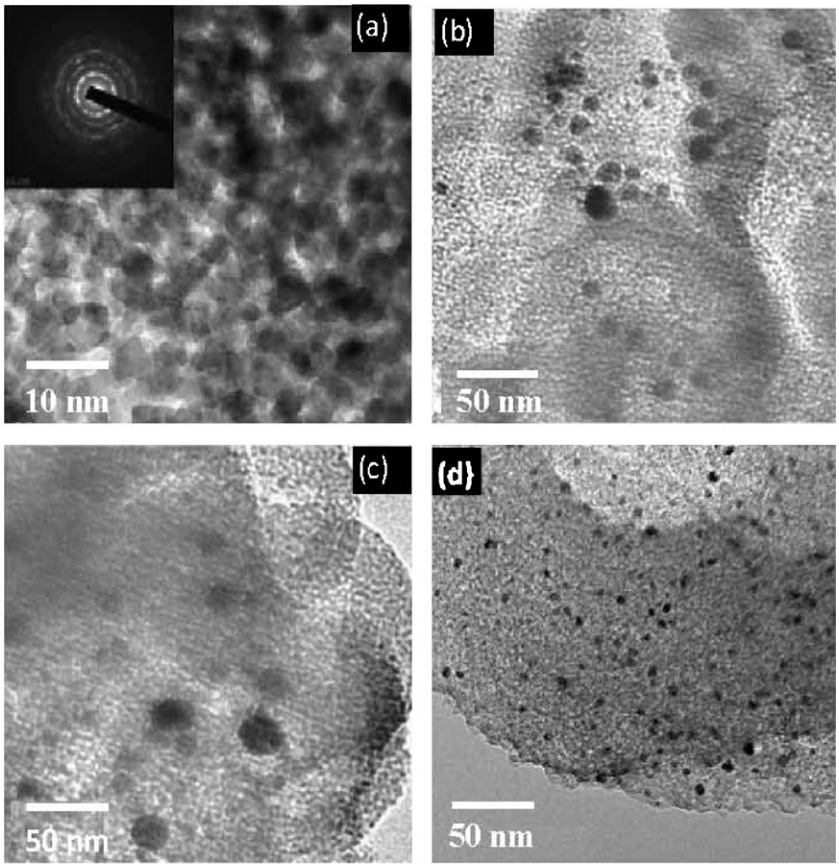

Fig. 4. TEM images of hexagonal mesoporous Pt/TiO_2 nanocomposites calcined at 500 (a), 600 (b) and 700 °C (c) and Pt/TiO_2 Degussa.

2. The systems Pt (500–700 °C) exhibited the highest photocatalytic activities of the hexagonally mesostructured Pt/TiO_2 nanocomposites with respect to the other investigated systems (Pt-25 and P-25).
3. From the economic point of view, ordered mesochannels prepared upon calcination at 600 °C are considered to be the optimum for saving energy in the photocatalyst preparation without much loss of photocatalytic performance.

Furthermore, a series of experiments has been carried out to study the effect of catalyst loading (Pt-600) on CO removal efficiency under the aforementioned conditions at CO concentration of about 400 ppmV displayed in Fig. 7.

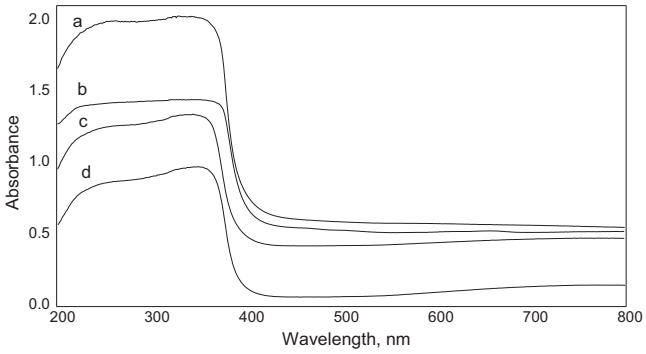

Fig. 5. UV–vis absorption spectrum of Pt-500 (a), Pt-600 (b) Pt-700 (c) and Pt-25 (d).

The features emerge from the results of CO % versus catalyst loading are as follows:

1. An increase in the catalyst weight from 0. 15 to 0.4 g, leads to an increase of CO removal efficiency from 89.2 to 100% respectively.
2. While at catalyst loading more than 0.35 g, the CO removal efficiency almost remains unchanged, accordingly the optimum

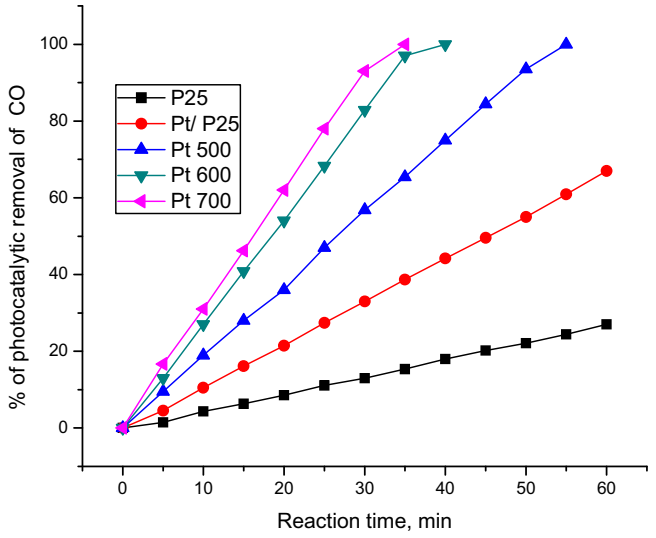

Fig. 6. Photooxidation of CO over P-25 and synthesised photocatalysts (Pt-500, Pt-600, Pt-700 and Pt-25).

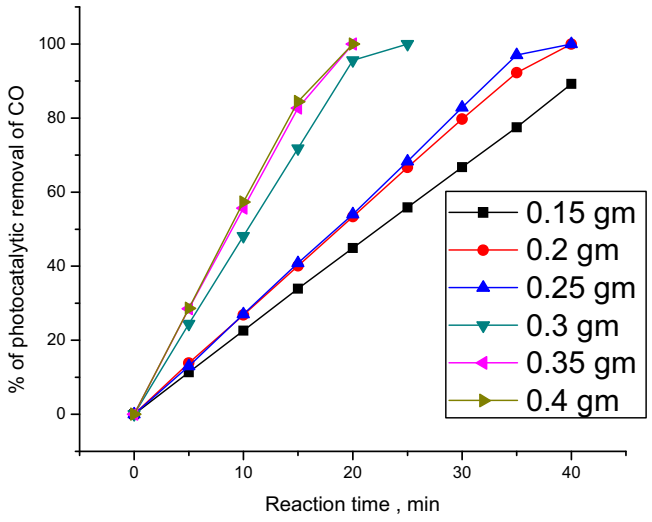

Fig. 7. Photooxidation of CO over different loading (g) of Pt-600.

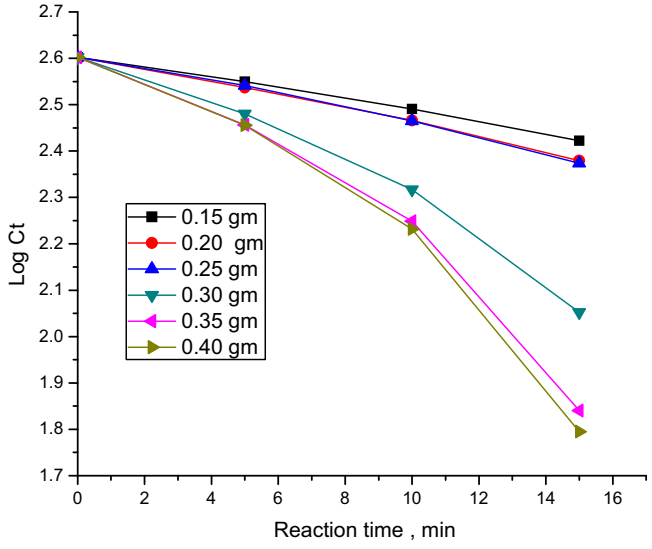

Fig. 8. Kinetics for the photooxidation of CO over different loading of Pt-600.

condition of catalyst weight is 0.35 g for the most effecient removal of CO (100%).

The reaction order with respect to CO was determined by plotting the reaction time (t) versus the Log $[C]_t$ [8]; according to the following equation for various Pt-600 loading

$$\text{Log}\,[C]_t = -kt + \text{Log}\,[C]_0$$

where $[C]_t$ and $[C]_0$ represent the concentration (ppm) of the substrate in solution at zero and t time (min) of illumination respectively, k represents the apparent rate constant (min^{-1}) (Fig. 8 and Table 3).

The results show that the reaction followed first order kinetics with respect to CO and the rate constants were ranging from 132×10^{-4} to $465 \times 10^{-4}\,\text{min}^{-1}$.

The first order rate equation for CO given by:

$$R = k[\text{CO}]$$

Table 3
Apparent rate constant k ($\text{min}^{-1} \times 10^{-4}$) at different Pt-600 loadings (g).

Pt-600 loading (g)	k ($\text{min}^{-1} \times 10^{-4}$)
0.15	132
0.20	159
0.25	161
0.30	350
0.35	488
0.40	464

4. Conclusions

In summary, the mesoporous platinum doped titania photocatalysts exhibit much higher efficiency for the photooxidation of carbon monoxide than commercial TiO_2 Degussa P-25 and Pt photodeposited on commercial TiO_2 Degussa under UV irradiation due to the higher efficiency of generation and separation of photoinduced electrons and holes in the former than those in the latter. The reaction followed first order kinetics with respect to CO and the rate constants ranged from 132×10^{-4} to $465 \times 10^{-4}\,\text{min}^{-1}$ by changing loading from 0.15 to 0.4 g respectively. The CO_2 formation rate increase is a good evidence for superior photocatalytic oxidation efficiencies within the mesoporous Pt/TiO_2 system to that of Pt/ TiO_2 Degussa.

References

[1] J. Ovenstone, J. Mater. Sci. 36 (2001) 1325.
[2] B. Xin, L. Jing, Z. Ren, B. Wang, H. Fu, J. Phys. Chem. B 109 (2005) 2805.
[3] L. Ge, M.X. Xu, Mater. Sci. Eng. B 131 (2006) 222.
[4] C. Hu, Y. Lan, J. Qu, X. Hu, A. Wang, J. Phys. Chem. B 110 (2006) 4066.
[5] S.C. Chan, M.A. Barteau, Langmuir 21 (2005) 5588.
[6] H. Yang, K. Zhang, R. Shi, X. Li, X.i. Dong, Y. Yu, J. Alloys Compd. 413 (2006) 302.
[7] J. Ma, L. -Sheng Qiang, H. Yang Li, X. Bo Tang, Sci. Adv. Mater. 2 (2010) 539.
[8] Y. Tokunaga, H. i Uchiyama, Y. Oaki, H. Imai, Sci. Adv. Mater. 2 (2010) 69.
[9] Y. Liao, W. Que, Z. Tang, W. Wang, W. Zhao, J. Alloys Compd. 509 (2011) 1054.
[10] 1.K.L. Yeung, S.T. Yau, A.J. Maira, J.M. Coronado, J. Soria, P.L. Yue, J. Catal. 219 (1) (2003) 107.
[11] K.L. Yeung, A.J. Maira, J. Stolz, E. Hung, N.K.C. Ho, A.C. Wei, J. Soria, J. Chao, J. Phys. Chem. B 106 (18) (2002) 4608.
[12] A.J. Maira, W.N. Lau, C.Y. Lee, P.L. Yue, C.K. Chan, K.L. Yeung, Chem. Eng. Sci. 58 (3–6) (2003) 959.
[13] S.L. Cao, K.L. Yeung, P.L. Yue, Appl. Catal. B 76 (1–2) (2007) 64.
[14] S.L. Cao, K.L. Yeung, P.L. Yue, Appl. Catal. B 68 (3–4) (2006) 99.
[15] R.M. Mohamed, M.A. Al-Rayyani, E.S. Baeissa, I.A. Mkhalid, J. Alloys Compd. 509 (2011) 6824.
[16] R.M. Mohamed, I.A. Mkhalid, J. Alloys Compd. 501 (2010) 301.
[17] R.M. Mohamed, I.A. Mkhalid, J. Alloys Compd. 501 (2010) 143.
[18] F. Boccuzzi, A. Chiorino, M. Manzoli, Mater. Sci. Eng. C 15 (2001) 215.
[19] K.Y. Ho, K.L. Yeung, J. Catal. 242 (1) (2006) 131.
[20] K.Y. Ho, K.L. Yeung, Gold Bull. 40 (1) (2007) 15.
[21] S. Chen, R.W. Murray, J. Phys. Chem. B 103 (1999) 9996.
[22] V. Subramanian, E.E. Wolf, P.V. Kamat, J. Phys. Chem. B 107 (2003) 7479.
[23] T. Hirakawa, P.V. Kamat, Langmuir 20 (2004) 5645.
[24] H.J. Zhang, X.Y. Li, G.H. Chen, J. Mater. Chem. 19 (2009) 8223.
[25] O. Carp, C.L. Huisman, A. Reller, Prog. Solid State Chem. 32 (2004) 33.
[26] S. Hwang, M.C. Lee, W. Choi, Appl. Catal. B: Environ. 46 (1) (2003) 49.
[27] A.V. Vorontsov, E.N. Savinov, J. Zhensheng, J. Photochem. Photobiol. A: Chem. 125 (1–3) (1999) 113.
[28] S. Gan, Y. Liang, D.R. Baer, M.R. Sievers, G.S. Herman, C.H.F. Peden, J. Phys. Chem. B 105 (12) (2001) 2412.
[29] M.R. Hoffmann, S.T. Martin, W. Choi, D.W. Bahnemann, Chem. Rev. 95 (1) (1995) 69.
[30] O. Legrini, E. Oliveros, A.M. Braun, Chem. Rev. 93 (2) (1993) 671.
[31] E. Allain, S. Besson, C. Durand, M. Moreau, T. Gacoin, J.P. Boilot, Adv. Funct. Mater. 17 (4) (2007) 549–554.
[32] I. Bannat, K. Wessels, T. Oekermann, J. Rathousky, D. Bahnemann, M. Wark, Chem. Mater. 21 (8) (2009) 1645.
[33] C. Wang, J. Rabani, D.W. Bahnemanna, J.K. Dohrmann, J. Photochem. Photobiol. A: Chem. 148 (2002) 169.
[34] I. Othman, R.M. Mohamed, I.A. Ibrahiem, M.M. Mohamed, Appl. Catal. A 299 (2006) 95.

[35] J. Thomas, K. Praveen Kumar, S. Mathew, Sci. Adv. Mater. 2 (2010) 481.
[36] J. Thomas, K. Praveen Kumar, S. Mathew, Sci. Adv. Mater. 3 (2011) 59.
[37] K. Shimasaki, N. Suzuki, N. Miyamoto, Y. Yamauchi, J. Nanosci. Nanotechnol. 11 (2011) 3256.
[38] H. Luo, C. Wang, Y. Yan, Chem. Mater. 15 (2003) 3841.
[39] JCPDS PDF-2 Pattern 01-076-1935.
[40] H. Einaga, A. Ogata, S. Futamura, T. Ibusuki, Chem. Phys. Lett. 338 (4–6) (2001) 303.
[41] T. Ji, L. Dong, Y. Liu, L. Li, B. Sun, J. Nanosci. Nanotechnol. 11 (2011) 3861.
[42] Y. Xiong, J. Chen, B. Wiley, Y. Xia, Y. Yin, Z.-Y. Li, Nano Lett. 5 (7) (2005) 1237.